Indian Journal of Chemistry
Vol. 58A, January 2019, pp. 9-17

A fluorescent zinc(II)-based layered complex for selective sensing of $Cr_2O_7^{2-}$ and Fe^{3+} ions in water system

De-Yu Zhang, Hongming He, Yu Zhang, Xiu-Guang Wang*, Xiao-Jun Zhao* & En-Cui Yang*

College of Chemistry, Key Laboratory of Inorganic-Organic Hybrid Functional Material Chemistry, Ministry of Education, Tianjin Key Laboratory of Structure and Performance for Functional Molecules, Tianjin Normal University, Tianjin 300387, People's Republic of China

Email: encui_yang@163.com (ECY)/ hxxywxg@mail.tjnu.edu.cn (XGW)/ xiaojun_zhao15@163.com (XJZ)

Received 27 August 2018; revised and accepted 17 December 2018

A new Zn(II)-organic framework with 2,2-bipyridine-5,5-dicarboxylate (bpydc) ligand $\{[Zn(H_2O)(bpydc)]\cdot CH_3OH\}_n$ has been obtained solvothermally, followed by structural and photophysical characterization. Structural analysis reveals that the distorted Zn^{2+} octahedra are periodically extended by the ditopic $bpydc^{2-}$ connector, leading to a coplanar grid-like (4 4) layer. The complex exhibits excellent thermal and environmental stability as well as good dispersion in water system. More interestingly, resulting from the efficient ligand to metal charge transfer, the complex has been observed to emit strong blue emission dispersed in water medium enabling the detection of both $Cr_2O_7^{2-}$ and Fe^{3+} ions through fluorescence quenching with large quenching constants (1.12×10^5 M^{-1} and 2.12×10^4 M^{-1}) and low limits of detection (0.54 μM and 1.02 μM). These interesting results suggest that the complex can potentially serve as a promising dual-responsive luminescent sensor material for environmental pollutant monitoring.

Keywords: Coordination polymers, Crystal structures, Solvothermal reactions, Fluorescence sensor materials, Quenching effects

Luminescent transition metal-based coordination polymers (CPs) have recently gained great interest due to their intriguing structural diversity and promising photophysical properties[1-3]. These interesting CPs with excellent stability, quick fluorescence response and strong emission intensity have been widely used as luminescence chemosensors for discriminating inorganic toxic cations, heavy metal ions, volatile organic gases, antibiotics and nitroaromatic explosives. Especially, some intense fluorescence emissions can be clearly observed by the naked eye, which greatly advance practicality and simplicity of operations of these functional materials[4]. To date, lots of luminescence Zn^{2+}, Cd^{2+}, Mg^{2+} and Ir^{2+} based CPs with variable dimensionality and intriguing structures have been prepared and incorporated with carboxylate-modified conjugated aromatic ligands, exhibiting bright luminescence resulting from the efficient ligand-to-metal charge transfer (LMCT) and are applied to detect Fe^{3+}, Al^{3+}, Hg^{2+}, $Cr^{+3/+4}$, CN^-, procaine, motin, 6-mercaptopurine anticancer drug, picric acid and so on[5-12]. It has been found that the sensing capacity is closely related with multiple Lewis basic sites[13], additional chelating NH_2 sites[14,15], interesting guest encapsulate[16] and so on[17].

On the other hand, environmental and ecological pollution to air, water and soil are on the rise. These pollution concerns have significantly damaged human health and sustainable development[18]. Great efforts and a huge amount of money are thus being invested by both governments and scientists to overcome environmental issues. The two environmental contaminants, $Cr_2O_7^{2-}$ anion and Fe^{3+} cation are persistent pollutants. $Cr_2O_7^{2-}$ has become one of the most serious environmental non-biodegradable contaminants and is listed as a priority pollutant by the U.S. Environmental Protection Agency. An excess and/or abnormal distribution of $Cr_2O_7^{2-}$ and/or Fe^{3+} ions at trace or even ultra-trace levels can induce DNA damage, posing a serious threat to human health and the natural environment, resulting in various serious disorders (skin diseases, iron deficiency anemia, agrypnia, and decreased immunity) and several diseases such as Alzheimer's, Huntington's, and Parkinson's diseases. Therefore, it is necessary and urgent to conveniently and quickly detect the occurrence and completely remove the two serious pollutants from water medium. At present, commonly used methods for the identification of $Cr_2O_7^{2-}$ and Fe^{3+} ions such as atomic absorption spectrometry,

atomic emission spectrometry, ICP-MS, XRF, gas chromatography, mass spectrometry, atomic force microscopy and ion-selective electrodes[19] generally require complicated measurement instruments and large amounts of consumption of cryogen and solvent[20,21]. Hence, the challenge exists for developing new methods having high efficiency and easy handling in order to detect trace amounts of $Cr_2O_7^{2-}$ and Fe^{3+} ions in aqueous medium. Herein, the self-assembly of 2,2′-bipyridine-5,5′-dicarboxylic acid (H_2bpydc) ligand and Zn^{2+} ion, generated a new layered CP under solvothermal conditions, which was further used as a fluorescent probe to recognize $Cr_2O_7^{2-}$ and Fe^{3+} pollutants. To the best of our knowledge, only a limited number of metal complexes with Co^{2+}, Ni^{2+} and Zn^{2+} centers and N-heterocyclic coligands have been reported, and no fluorescent sensing behavior have been investigated so far[22–26]. Fluorescent Zn^{2+} ion can greatly enhance the emission intensity by coordination with the conjugated $bpydc^{2-}$ connectors responsible for the possible multiple-responsive sensing ability. Herein, solvothermal synthesis, crystal structure and dual-responsive ion-sensing behavior of the layered complex have been reported.

Materials and Methods

Organic ligand H_2bpydc was synthesized by a slightly modified method[22,26]. Other analytical grade reagents were commercially obtained from either Acros or Tianjin Chemical Reagent Factory and used without further purification. Elemental analyses of C, H and N were performed by a Leeman-Labs CE-440 analyzer. Fourier transform FT-IR spectra (KBr pellets) of the complex was collected on Nicolet Avatar-370 spectrometer in the range 400–4000 cm^{-1}. Thermogravimetric analysis (TGA) was performed on a Shimadzu simultaneous DTG-60A compositional analysis instrument in the range 25–800 °C under a N_2 atmosphere at a heating rate of 5 °C min^{-1}. The powder X-ray diffraction (PXRD) patterns were obtained by Rigaku D/max-2500 diffractometer at 60 kV and 300 mA with Cu-Kα radiation (λ = 1.5406 Å), at a scan speed of 0.2° min^{-1} and step size of 0.02° in 2θ. The simulated PXRD pattern was calculated with the single-crystal X-ray diffraction data and processed using the free Mercury v1.4 program provided by the Cambridge Crystallographic Data Center to calculate the simulated PXRD pattern. Fluorescence spectra of the obtained samples were recorded on a F-4600 fluorescence spectrophotometer from Hitachi at room temperature. UV-vis spectra of the inorganic anions and cations were obtained using a UV-2700 spectrophotometer.

Synthesis of 1

$Zn(NO_3)_2·6H_2O$ (30.0 mg, 0.10 mmol) and H_2bpydc (10.0 mg, 0.04 mmol) were dissolved in mixed solvents containing MeOH (3.0 mL), N,N′-dimethylacetamide (DMA, 3.0 mL) and doubly deionized water (0.5 mL). The pH value of the initial mixture was slowly adjusted to ca 8 with aqueous NaOH solution (2.0 M). Then, the resulting mixture was transferred and sealed in a Teflon-lined stainless steel vessel (23.0 mL), and heated at 100 °C for 3 days. After the mixture was cooled to room temperature at a rate of 7 °C h^{-1}, colorless block-shaped single crystals suitable for X-ray diffraction analyses were obtained directly. Yield: 66% on the basis of H_2bpydc ligand. Calcd for $C_{13}H_{12}N_2O_6Zn$: C, 43.66; H, 3.38; N, 7.83%. Found: C, 43.64; H, 3.40; N, 7.81%. FT-IR (KBr pellet, cm^{-1}): 3374 (br), 3055 (w), 1614 (s), 1552 (s), 1428(s), 1381 (s), 1225 (w), 1164 (w), 1138 (w), 1033 (m), 879 (m), 849 (m), 773 (m),709 (m), 571 (w).

X-ray single-crystal data collection and structure determination

Diffraction intensity of **1** was collected on a computer controlled Bruker APEX-II CCD diffractometer equipped with graphite-monochromated Mo-Kα radiation with a radiation wavelength of 0.71073 Å using the φ-ω scan technique at 296 K. There was no evidence of crystal decay during the data collection. Semiempirical multi-scan absorption corrections were performed for all data with SADABS[27] and the program SAINT[28] was used for integration of the diffraction profiles. The structure was solved by direct methods and refined with the full-matrix least-squares technique using the SHELXS-97 and SHELXL-2014/7 programs[29]. Anisotropic thermal parameters were assigned to non-hydrogen atoms. The crystallographic data and selected bond lengths and angles for **1** are given in Table 1 and Table 2, respectively.

Luminescent sensing experiments

The stock suspension of **1** (0.1 mg mol^{-1}) was prepared by introducing 10.0 mg of crystalline sample of **1** into 100.0 mL water. The emission spectra of the stock suspension were recorded in the absence and presence of selected inorganic anions (I^-, NO_3^-, BrO_3^-, F^-, CrO_4^-, MnO_4^-, ClO_3^- and $Cr_2O_7^{2-}$, 1×10^{-3} mol L^{-1}) or cations (Ag^+, Pb^{2+}, Zn^{2+}, Na^+, Al^{3+}, K^+,

Li^+ and Fe^{3+}, 1×10^{-3} mol L^{-1}). Luminescent titration experiments were performed by collecting the emission intensity of the stock suspension in the absence and presence of various concentrations of $Cr_2O_7^{2-}$ (1×10^{-3} mol L^{-1}) and Fe^{3+} (1×10^{-3} mol L^{-1}) respectively.

Results and Discussion

Synthesis and FT-IR spectrum

Complex **1** was solvothermally prepared in a ternary solvent system (CH_3OH-DMA-H_2O), in which the volume ratio of the mixed solvents and the pH value of the reaction medium are found to be important for the generation of the crystalline product. Additionally, complex **1** is air-stable and insoluble in common organic solvents.

Table 1 — Crystal and structure refinement data for **1**

CCDC No.	1852758
Empirical formula	$C_{13}H_{12}N_2O_6Zn$
Formula weight	357.62
Crystal size (mm)	0.220 × 0.210 × 0.180
Crystal system	monoclinic
space group	$P2_1/n$
a (Å)	10.9332(8)
b (Å)	9.7267(7)
c (Å)	12.5808(10)
β (º)	92.442(2)
V (Å^3)	1336.68(17)
Z, D_c (g cm^{-3})	4, 1.777
h / k / l	–10, 13 / –12, 11 / –15, 12
F (000)	728
μ (mm^{-1})	1.871
reflections collected / unique	8505 / 2764
R_{int}	0.0263
data / restraints / params	2764 / 0 / 201
R_1[a], wR_2[b] [$I > 2\sigma$ (I)]	0.0259, 0.0637
R_1, wR_2 [all data]	0.0320, 0.0656
GOF on F^2	1.068
$\Delta\rho_{max}$, $\Delta\rho_{min}$ [e Å^{-3}]	0.348, –0.389

[a] $R_1 = \Sigma(||F_o|-|F_c||)/\Sigma|F_o|$; [b] $wR_2 = [\Sigma w(|F_o|^2-|F_c|^2)^2/\Sigma w(F_o^2)^2]^{1/2}$

Table 2 — Selected bond lengths (Å) and angles (°) for **1**

Zn(1)–O(1)[a]	2.0000(15)	Zn(1)–N(1)	2.1352(17)
Zn(1)–O(5)	2.0681(15)	Zn(1)–O(3)[b]	2.2256(16)
Zn(1)–N(2)	2.1164(16)	Zn(1)–O(4)[b]	2.2568(17)
O(1)[a]–Zn(1)–O(5)	92.81(7)	N(2)–Zn(1)–O(3)[b]	93.83(6)
O(1)[a]–Zn(1)–N(2)	97.45(7)	N(1)–Zn(1)–O(3)[b]	89.06(6)
O(5)–Zn(1)–N(2)	95.25(6)	O(1)[a]–Zn(1)–O(4)[b]	110.00(6)
O(1)[a]–Zn(1)–N(1)	91.17(7)	O(5)–Zn(1)–O(4)[b]	93.39(6)
N(2)–Zn(1)–N(1)	76.73(6)	N(1)–Zn(1)–O(4)[b]	92.34(6)
O(5)–Zn(1)–O(3)[b]	88.55(6)	O(3)[b]–Zn(1)–O(4)[b]	58.48(6)

[a] Symmetry codes: [a]3/2 – x, y –1/2, 3/2 – z; [b]1/2 – x, y + 1/2, 3/2 – z.

In the FT-IR spectrum of **1**, a strong and broad band at 3374 cm^{-1} is attributed to the stretching vibrations of –OH, suggesting the presence of water and/or methanol molecules. As compared with the free H_2bpydc ligand, an absence of a characteristically strong peak at 1694 cm^{-1} in **1** is due to the full deprotonation of the organic ligand[30]. The characteristic bands for the asymmetric and symmetric stretching vibrations of the deprotonated carboxylate group are located at 1614, 1552 and 1428 1381 cm^{-1}. Thus, the IR results of **1** are in good agreement with that of single-crystal structural determination.

Crystal structure of 1

Single-crystal structural analysis shows that **1** crystallizes in the monoclinic $P2_1/n$ space group (Table 1), exhibiting a two-dimensional (2D) coplanar layer with distorted Zn^{2+} octahedra extended by doubly deprotonated bpydc^{2-} connectors. The asymmetric unit of **1** consists of one Zn^{2+} ion, one terminally coordinated water molecule, one doubly deprotonated bpydc^{2-} anion for charge compensation, as well as one lattice methanol molecule. As shown in Fig. 1a, the sole Zn^{2+} ion in **1** is encompassed by N_2O_4

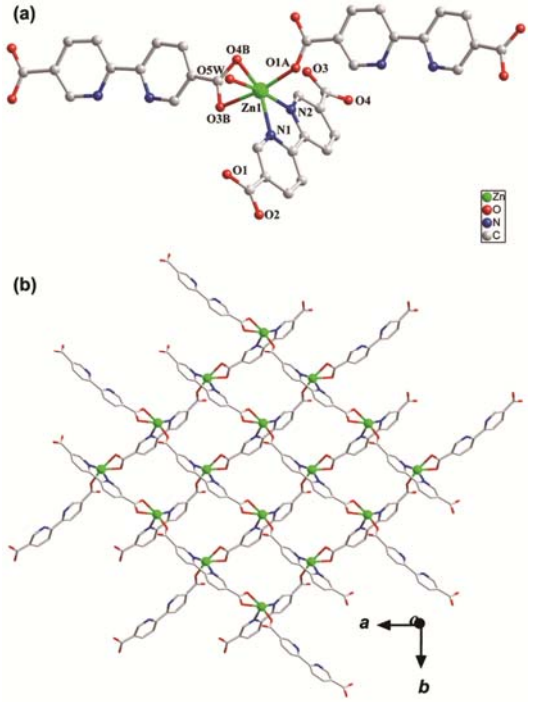

Fig. 1 — (a) Local coordination environment of Zn^{2+} ion in **1** (H atoms are omitted for clarity; symmetry codes: A = 3/2 – x, y – 1/2, 3/2 – z; B = 1/2 – x, y + 1/2, 3/2 – z; C = 3/2 – x, y + 1/2, 3/2 – z; D = 1/2 – x, y – 1/2, 3/2 – z), and, (b) Layered structure of **1** with distorted Zn^{2+} octahedra extended by bpydc^{2-} connectors in the crystallographic *ac* plane.

donors, three carboxylate O and two pyridyl N donors from three separate $bpydc^{2-}$ anions and one terminally coordinated water molecule, adopting a distorted octahedral coordination configuration. The bond lengths of Zn–O and Zn–O vary between 2.000(15) and 2.256(17) Å (Table 2), which are comparable with the Zn^{2+} based complexes with carboxylate and/or pyridyl ligands[23,24,31]. The $bpydc^{2-}$ ligand in **1** is in a doubly deprotonated form, affording its two pyridyl N and three carboxylate O donors to coordinate with Zn^{2+} ion in a pentadentate chelating bridging mode.

As illustrated in Fig. 1b, the adjacent Zn^{2+} ions are periodically bridged by the pentadentate $bpydc^{2-}$ connectors through two pyridyl N and three carboxylate O donors, leading to a coplanar (4 4) grid-like layer with the intralayer $Zn^{2+}\cdots Zn^{2+}$ distances of 7.8202(5) and 7.0974(5) Å. The adjacent 2D layers of **1** are stacked together through the popular O–H···O hydrogen bonding interactions between the coordinated water molecule and deprotonated carboxylate group of $bpydc^{2-}$ ligand (Supplementary Data, Table S1), resulting in a three-dimensional (3D) supramolecular network of **1** with the interlayer distance of 4.9896(5) Å (Supplementary Data, Fig. S1).

TG and PXRD patterns of 1

Compositional and thermal stability of the layered complex were investigated by the combined techniques of TGA measurement and variable-temperature PXRD patterns. TGA curve (Supplementary Data, Fig. S2) indicated that the first weight loss process of **1** occurred at room temperature and finished at 89 °C, corresponding to the release of the coordinated water molecule (obsd 6.0%, calcd 5.0%). Then, the second weight loss stage for the removal of lattice methanol molecule (obsd 10.3%, calcd 9.0%) was between 140 °C and 286 °C. Once the temperature is higher than 328 °C, the organic ligand of **1** was broken, which was not completely finished until 800 °C.

Phase purity and structural consistency of the bulk as-synthesized product were further confirmed by the well matched simulated and experimental PXRD patterns. The PXRD pattern of **1** after heating at 90 °C for 4h was the same as that of the simulated one (Fig. 2). However, the PXRD pattern of **1** after heating at 150 °C for 4 h was much different from the simulated one, suggesting that the layered framework of **1** was highly stable below 90 °C. The results of the variable-temperature PXRD patterns were consistent with the TG result. The water stability of **1** was also investigated by soaking the resultant sample in boiling water for ten days. The PXRD pattern of **1** after soaking was the same as that of the simulated one. These interesting results illustrate that **1** has high thermal stability and robustness water, which are important for the feasible applications of the functional materials.

Emission behavior of 1

Photoluminescence emission of **1** and free H_2bpydc ligand were respectively monitored in the solid-state at room temperature. As illustrated in Fig. 3, upon excitation at 381 nm, the isolated H_2bpydc molecule displays two broad emission bands centered at 411 nm and 551 nm. The two emissions are presumably due to the $\pi \rightarrow \pi^*$ and/or $n \rightarrow \pi^*$

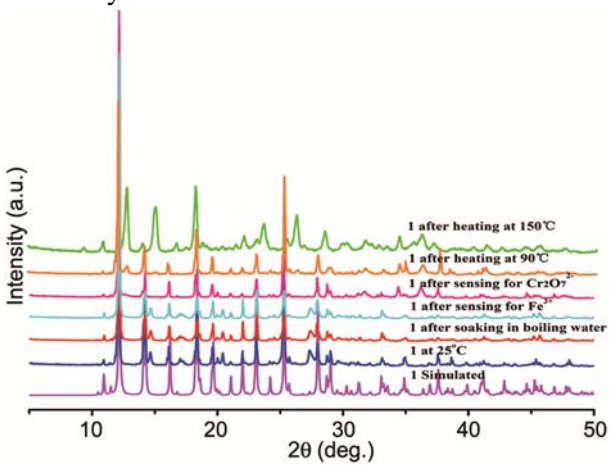

Fig. 2 — PXRD patterns of **1** upon different external stimuli.

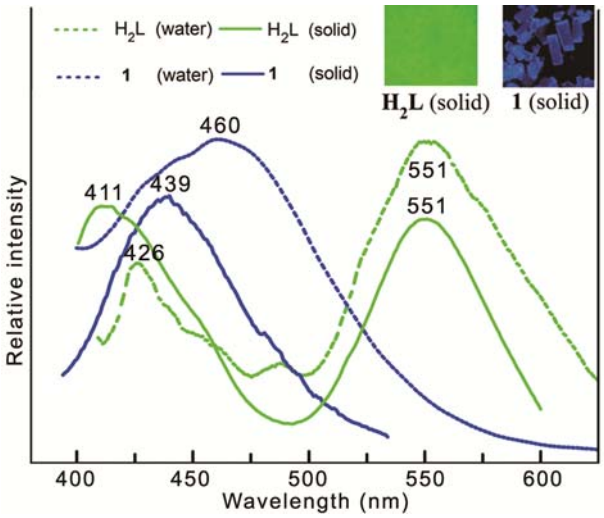

Fig. 3 — Excitation (dashed) and emission (solid) spectra of **1** and H_2bpydc in the solid-state and in water phase.

transitions of the aromatic dicarboxylatic acid. Upon excitation at 359 nm, complex **1** in the solid state shows a broad emission band centered at 439 nm. As compared with the luminescence of the H_2bpydc ligand, the emission of **1** has a considerable blue shift resulting from the coordination behavior of bpydc^{2-} to Zn^{2+} ion. Additionally, the intense emissions of H_2bpydc and **1** can be clearly observed by the naked eye under the irradiation of UV light at 365 nm, which exhibit bright green and blue emission signals (Fig. 3).

Selective sensing towards $Cr_2O_7^{2-}$ and Fe^{3+}

Complex **1** with intense blue emission can provide a suitable platform for the luminescence sensing of pollutants in nature. To explore the sensing ability of **1**, the emission behavior of **1** dispersed in water phase was evaluated. As compared with the emission in the solid state, the intense emission of **1** dispersed in water shifts to 460 nm upon excitation at 358 nm due to the solvent effect (Fig. 3), which can be used as a characteristic band to probe the toxic ions or molecules. Additionally, the solvent effect can also be confirmed by the emission of free organic ligand, in which the first emission of H_2bpydc is shifted from 411 nm in the solid state to 426 nm in the water system.

As shown in Fig. 4a, the fluorescence intensity of **1** at 460 nm is decreased to different extents in the presence of typically inorganic anions including I^-, NO_3^-, F^-, MnO_4^-, ClO_3^-, BrO_3^-, CrO_4^- and $Cr_2O_7^{2-}$. Especially, a drastic luminescent quenching of **1** is

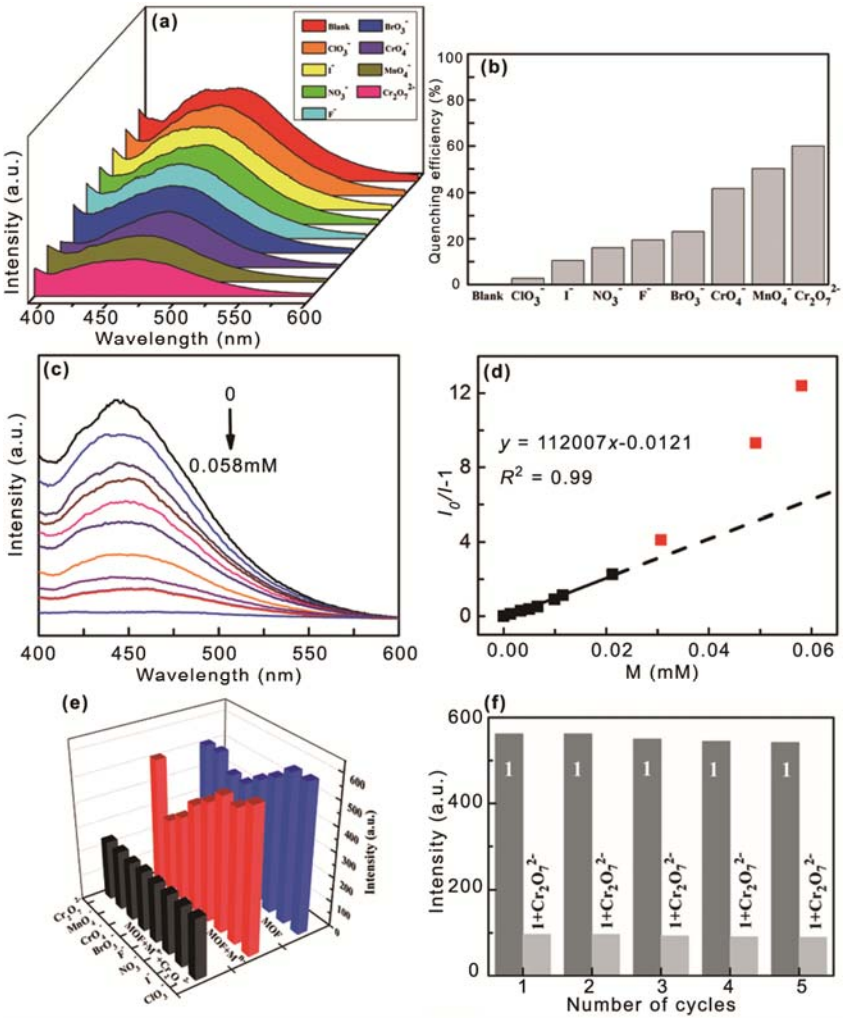

Fig. 4 — (a) Emission spectra of **1**-H_2O suspension in the presence of the indicated anions upon excitation at 359 nm. (b) Quenching percentage of **1**-H_2O at 460 nm by the indicated anions. (c) Luminescent intensity of **1**-H_2O suspension at different $Cr_2O_7^{2-}$ concentrations. (d) Plot of (I_0/I–1) versus concentration of $Cr_2O_7^{2-}$. (e) Luminescent intensity of **1**-H_2O suspension at 460 nm in the presence of the mixed-metal anions. (f) Luminescent intensity of **1**-H_2O suspension at 460 nm in the absence and presence of $Cr_2O_7^{2-}$ anion for each cycle test.

clearly observed by the addition of $Cr_2O_7^{2-}$ anion. Quenching efficiency ($(I_0–I)/I_0$) can be quantitatively evaluated by monitoring the intensity change of the emission peak. The quenching efficiency of **1** by $Cr_2O_7^{2-}$ anion is 60.0%, while the quenching efficiency of **1** by the other studied anions are much low (2.8% ~50.2%, Fig. 4b). These data suggest that **1** can selectively recognize $Cr_2O_7^{2-}$ anion in aqueous solution via luminescent quenching.

To quantitatively understand the strength of **1** towards $Cr_2O_7^{2-}$ anion, luminescence titration has been carried out with the gradual addition of aqueous $Cr_2O_7^{2-}$ solution (1.0 mM) to the emulation of **1** (0.1 mg mL^{-1}). As shown in Fig. 4c, the intensity of **1** at 460 nm decreases gradually with the increasing concentration of $Cr_2O_7^{2-}$ anion. When the concentration of $Cr_2O_7^{2-}$ anion is 1.33 μM, the intensity of **1** at 460 nm is decayed by 10.9%. When the concentration of $Cr_2O_7^{2-}$ is 5.8×10^{-5} mol L^{-1}, the intensity of **1** at 460 nm is almost totally quenched (Fig. 4c).

Quantitatively, the quenching effect of $Cr_2O_7^{2-}$ to **1** can be rationalized by the Stern-Volmer (S-V) equation: $(I_0/I) = K_{sv}$ [M] + 1, where I_0 and I are luminescent intensity of **1** suspension before and after the addition of $Cr_2O_7^{2-}$ anion respectively; [M] is the molar concentration of the $Cr_2O_7^{2-}$ anion, and K_{sv} is the quenching constant[32]. As shown in Fig. 4d, a good linear correlation is observed for the plot of $(I_0/I - 1)$ versus $[Cr_2O_7^{2-}]$ over the concentration range from 0 to 2.67×10^{-5} mol L^{-1}. The linear variation at low concentration is mainly due to static quenching[32]. The linear regression of the plot to the S-V equation affords $K_{sv} = 1.12\times10^5$ M^{-1} with a correlation coefficient (R^2) of 0.99. Limit of detection (LOD) can be further calculated from the $3\sigma/k$, in which σ (standard error) and k (slope) are extracted from the linear regression of I versus $[Cr_2O_7^{2-}]$, and the resulting value is 0.54 μM. The quenching constant of **1** towards $Cr_2O_7^{2-}$ is only slightly lower than that of $[Zn(2\text{-}NH_2bdc)(bibp)]_n$ and much higher than the Cd^{2+} based complexes (Table 3). These results reveal that the metal ions in the sensors play more important roles than those of the organic ligands.

The influence of other anions (I^-, NO_3^-, Br^-, MnO_4^-, ClO_3^-, BrO_3^- and CrO_4^-) on the detection of $Cr_2O_7^{2-}$ anion was also determined. The $Cr_2O_7^{2-}$ anion and the interfering anions were introduced sequentially one after the other, keeping the concentration of **1** constant at 0.1 mg mL^{-1}. The intensity of the emission at 460 nm was respectively monitored. As illustrated in Fig. 4e, each suspension shows similar fluorescence decaying in the presence of the interference ions, indicating that the addition of the other ions cannot significantly influence the highly sensitive and selective discrimination of **1** towards $Cr_2O_7^{2-}$ through decaying effect. Thus, complex **1** can be used as a sensor to detect $Cr_2O_7^{2-}$ anion in complicated water samples.

Luminescence detection ability of **1** to various cations (K^+, Na^+, Li^+, Zn^{2+}, Ag^+, Al^{3+}, Pb^{2+}, and Fe^{3+}) were also examined to explore the potentially multiple fluorescence responses. Interestingly, all the cations examined herein can weaken the luminescent intensity of **1** to some different degree (Fig. 5a), in which Fe^{3+} ion can cause a large drop in the luminescent intensity of the suspension implying a significant degree of quenching. The quenching percentage follows the order of Fe^{3+}> Al^{3+}> Pb^{2+}> Na^+ > Li^+> Ag^+> Zn^{2+}> K^+, implying that **1** can clearly distinguish Fe^{3+} among the eight typical ions examined herein (Fig. 5b).

The quenching constant of **1** by Fe^{3+} is quantitatively obtained by fluorescence titration

Table 3 — Quenching constants and detection limits of MOF-based luminescent sensors for $Cr_2O_7^{2-}$ and Fe^{3+}

Substrate	MOF	Medium	K_{sv} (M^{-1})	LOD(μM)
$Cr_2O_7^{2-}$	$[Zn(2\text{-}NH_2bdc)(bibp)]_n$[15]	water	6.5×10^6	-
	$\{[Cd(L)(BPDC)]\cdot2H_2O\}_n$[5]	water	6.4×10^3	37.6
	$\{[Cd(L)(SDBA)(H_2O)]\cdot0.5H_2O\}_n$[5]	water	4.97×10^3	48.6
	$[Cd_3\{Ir(ppy\text{-}COO)_3\}_2(DMF)_2(H_2O)_4]\cdot6H_2O\cdot2DMF$[17]	water	3.475×10^4	0.49
Fe^{3+}	FJI-C8[6]	DMF	8.24×10^3	23.3
	$\{[Cd(L)(BPDC)]\cdot2H_2O\}_n$[5]	water	3.63×10^4	2.21
	$\{[Cd(L)(SDBA)(H_2O)]\cdot0.5H_2O\}_n$[5]	water	3.59×10^4	7.14
	$[Cd_3\{Ir(ppy\text{-}COO)_3\}_2(DMF)_2(H_2O)_4]\cdot6H_2O\cdot2DMF$[17]	water	1.165×10^4	0.42

$2\text{-}NH_2bdc$ = 2-amino-1,4-benzenedicarboxylic acid; bibp = 4,4′-bis(imidazol-1-ylmethyl)-biphenyl; L = 4,4′-(2,5-bis-(methylthio)-1,4-phenylene)dipyridine; H_2BPDC = 4,4′-biphenyldicarboxylic acid; H_2SDBA = 4,4′-sulfonyldibenzoic acid, ppy-COOH = methyl-3-(pyridin-2-yl)benzoic acid.

experiment. As shown in Fig. 5c, the luminescent intensity of **1** is gradually reduced with the incremental addition of Fe^{3+} cation. When the concentration of Fe^{3+} is 0.28 mM, the intensity of **1** at 460 nm is almost totally quenched (Fig. 5c). A good linear correlation (R^2 = 0.99) between the quenching efficiency and the concentration of Fe^{3+} is observed below [Fe^{3+}] = 0.16 mM with $K_{sv} = 2.12\times10^4$ M^{-1} and R^2 = 0.99 (Fig. 5d). The LOD of **1** to Fe^{3+} is calculated to be 1.02 μM. The K_{sv} of **1** to Fe^{3+} is lower than the known Cd^{2+} derived complexes listed in Table 3, suggesting relatively weak affinity of Fe^{3+} to **1**. However, the LOD of **1** is better than those of three complexes (FJI-C8, $\{[Cd(L)(BPDC)]\cdot2H_2O\}_n$ and $\{[Cd(L)(SDBA)(H_2O)]\cdot0.5H_2O\}_n$, Table 3).

The influence of other cations (K^+, Na^+, Li^+, Zn^{2+}, Ag^+, Al^{3+} and Pb^{2+}) on the response of **1** towards Fe^{3+} is examined by the same method described above. As compared with the quenching behavior of **1** by Fe^{3+}, each suspension shows similar fluorescence decaying after introducing the mixture containing Fe^{3+} and the interfering ion (Fig. 5e). These results indicate that the highly sensitive and selective recognization of Fe^{3+} by **1** is not influenced by the presence of other ions examined herein.

Reversibility of 1

Repeatability and regeneration are highly important for the feasible applications of the chemosensors[1]. Complex **1,** that is well dispersed in water system can

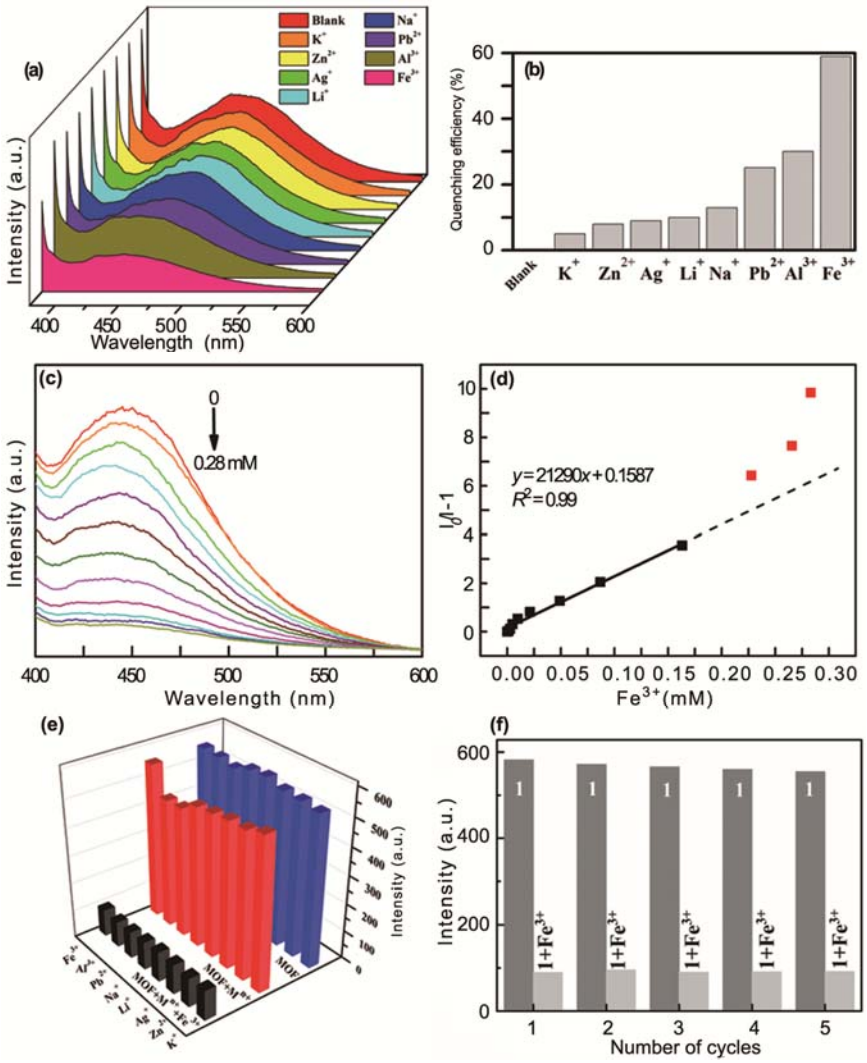

Fig. 5 — (a) Emission spectra of **1**-H_2O suspension in the presence of different cations upon excitation at 359 nm. (b) Quenching efficiency of **1**-H_2O suspension by different cations. (c) Luminescent intensity of **1**-H_2O suspension in different Fe^{3+} concentrations. (d) Plot of (I_0/I–1) versus concentration of Fe^{3+}. (e) Luminescent intensity of 1-H_2O suspension in the presence of different mixed-metal cations. (f) Luminescent intensity for the 460 nm of 1-H_2O suspension in the absence and presence of Fe^{3+} ion for each cycle test.

be easily recovered by simple centrifugation. Moreover, the luminescent intensity of regenerated sample is almost comparable with that of the freshly synthesized product (Fig. 4f and Fig. 5f). These recyclable experiments have confirmed that the sample can be continuously regained and reused to efficiently recognize $Cr_2O_7^{2-}$ and Fe^{3+} ions for at least five cycles. Thus, it can be concluded that complex **1** has good reproducibility and stability as a fluorescent probe.

Mechanism on luminescence quenching

To ensure the feasibility of the luminescence sensors, it is most important to understand the mechanism and origin of selective discrimination between the sensor and the pollutant. The PXRD pattern of the recyclable sample after five runs is well consistent with the simulated one (Fig. 2), indicating that the luminescence quenching is not caused by the collapse of the framework. By contrast, the absorption spectra of $Cr_2O_7^{2-}$ and Fe^{3+} show considerable overlap with the excitation spectrum of **1** (Fig. 6), while other selected cations and anions display negligible overlap with the excitation spectrum of **1**. Thus, the luminescent quenching is mainly attributed to the competitive absorption of excitation wavelength energy between **1** and the two pollutants. The favorable absorption of the $Cr_2O_7^{2-}$ or Fe^{3+} to the excitation energy weakens the charge transfer between the Zn^{2+} ion and 2,2-bipyridine-5,5-dicarboxylate ligand, leading to the fluorescence decay of the complex.

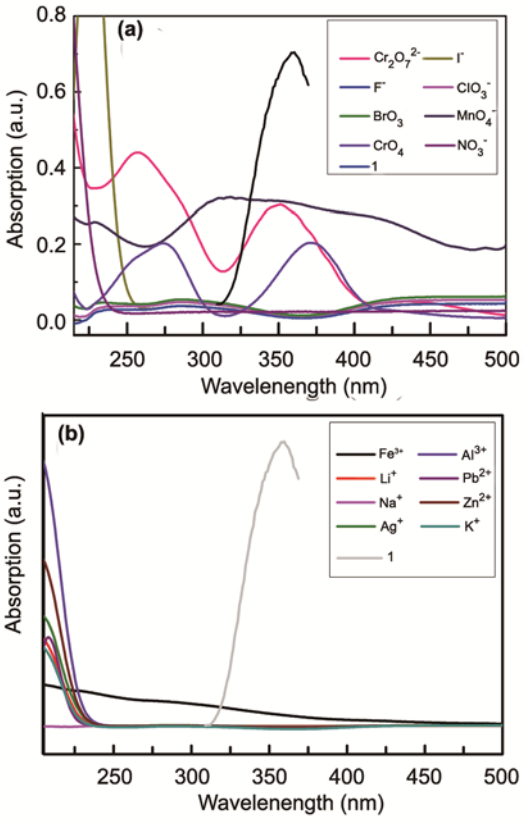

Fig. 6 — UV-vis absorption spectra of different analytes (1.0 mM) and excitation spectrum of **1**.

Conclusions

A fluorescence layered complex with Zn^{2+} octahedra extended by ditopic 2,2-bipyridine-5,5-dicarboxylate connectors was solvothermally prepared. The complex has significant advantages as a luminescent sensing material with good dispersion, high thermal and water stability as well as easy regeneration. More importantly, the complex can selectively recognize both $Cr_2O_7^{2-}$ and Fe^{3+} ions in water system by fluorescent quenching with quenching constants of 1.12×10^5 and 2.12×10^4 M^{-1} and limits of detection of 0.54 and 1.02 μM.

Supplementary Data

Crystallographic data for the structural analysis of complex **1** have been deposited with Cambridge Crystallographic Data Centre, under CCDC No. 1852758. Copy of this information may be obtained free of charge from: The Director, CCDC, 12 Union Road, Cambridge CB2 1EZ, UK (fax: 44-1223-336-033: Email: deposit@ccdc.cam.ac.uk). Other supplementary data associated with this article are available in the electronic form at http://www.niscair.res.in/jinfo/ijca/IJCA_58A(01)09-17_SupplData.pdf.

Acknowledgement

Financial supports from the National Natural Science Foundation of China (Grants 21571140, 21671149 and 21531005), the 973 Program (2014CB845601) and the Program for Innovative Research Team in University of Tianjin (TD13-5074) are gratefully acknowledged.

References

1 Kreno L E, Leong K, Farha O K, Allendorf M, Van Duyne R P & Hupp J T, *Chem Rev*, 112 (2012) 1105.
2 Heine J & Müller-Buschbaum K, *Chem Soc Rev*, 42 (2013) 9232.
3 Cui Y J, Yue Y F, Qian G D & Chen B L, *Chem Rev*, 112 (2012) 1126.
4 (a) He H M, Chen S H, Zhang D Y, Hao R, Zhang C, Yang E C & Zhao X J, *Dalton Trans*, 46 (2017) 13502;

(b) He H M, Chen S H, Zhang D Y, Yang E C & Zhao X J, *RSC Adv*, 7 (2017) 38871.

5 Chen S G, Shi Z Z, Qin L, Jia H L & Zheng H G, *Cryst Growth Des*, 17 (2017) 67.

6 Chen C, Wang X, Li L, Huang Y & Cao R, *Dalton Trans*, 47 (2018) 3452.

7 Xiao J N, Liu J J, Gao X C, Ji G F, Wang D B & Liu Z L, *Sens Actuators B*, 269 (2018) 164.

8 Wu Z F, Tan B, Feng M L, Lan A J & Huang X Y, *J Mater Chem A*, 2 (2014) 6426.

9 Nagarkar S S, Joarder B, Chaudhari A K, Mukherjee S & Ghosh S K, *Angew Chem Int Ed*, 52 (2013) 2881.

10 Singha D K & Partha M, *Inorg Chem*, 54 (2015) 6373.

11 Karmakar A, Kumar N, Samanta P, Desai A V & Ghosh S K, *Chem Eur J*, 22 (2016) 864.

12 (a) Gupta V K, Singh A K & Kumawat L K, *Sens Actuators B*, 195 (2014) 98; (b) Gupta V K, Atar N, Yola M L, Üstündag Z & Uzun L, *Water Res*, 48 (2014) 210; (c) Yola M L, Gupta V K, Eren T, Şen A E & Atar N, *Electrochim Acta*, 120 (2014) 204; (d) Gupta V K, Mergu N, Kumawat L K & Singh A K, *Sens Actuators B*, 207 (2015) 216; (e) Gupta V K, Mergu N, Kumawat L K & Singh A K, *Talanta*, 144 (2015) 80; (f) Karimi-Maleh H, Tahernejad-Javazmi F, Atar N, Yola M L, Gupta V K & Ensafi A A, *Ind Eng Chem Res*, 54 (2015) 3634; (g) Gupta V K, Sethi B, Sharma R A, Agarwal S & Bharti A, *J Mol Liq*, 177 (2013) 114; (h) Gupta V K, Karimi-Maleh H & Sadegh R, *Int J Electrochem Sci,* 10 (2015) 303.

13 Zhang H M, Yang J, Kan W Q, Liu Y Y & Ma J F, *Cryst Growth Des*, 16 (2016) 265.

14 Zhao D, Liu X H, Zhao Y, Wang P, Liu Y, Azam M, Al-Resayes S I, Lu Y & Sun W Y, *J Mater Chem A*, 5 (2017) 15797.

15 Wen L, Zheng X, Lv K, Wang C & Xu X, *Inorg Chem*, 54 (2015) 7133.

16 Lv R, Li H, Su J, Fu X, Yang B Y, Gu W & Liu X, *Inorg Chem*, 56 (2017) 12348.

17 Fan K, Bao S S, Nie W X, Liao C H & Zheng L M, *Inorg Chem*, 57 (2018) 1079.

18 (a) Gupta V K, Singh L P, Singh R, Upadhyay N, Kaur S P & Sethi B, *J Mol Liq*, 174 (2012) 11; (b) Gupta V K, Kumar S, Singh R, Singh L P, Shoora S K & Sethi B, *J Mol Liq*,195 (2014) 65; (c) Asfaram A, Ghaedi1a M, Agarwal S, Tyagib I & Gupta V K, *RSC Adv*, 5 (2015) 18438.

19 (a) Zdrenghea U V, Tomoaia G, Pop-Toader D V, Mocanu A, Horovitz O & Tomoaia-Cotisel M, *Comb Chem High Throughput Screening,* 14 (2011) 237; (b) Gupta V K, Ganjali M R, Norouzi P, Khani H, Nayak A & Agarwal S, *Crit Rev Anal Chem*, 41 (2011) 282; (c) Srivastava S K, Gupta V K & Jain S, *Analyst,* 120 (1995) 495; (d) Srivastava S K, Gupta V K, Dwivedi M K & Jain S, *Analytical Proceedings Including Anal Commun,* 32 (1995) 21; (e) Srivastava S K, Gupta V K & Jain S, *Anal Chem,* 68 (1996) 1272; (f) Karthikeyan S, Gupta V K, Boopathy R, Titus A & Sekaran G, *J Mol Liq*,173 (2012) 153; (g) Dehghani M H, Sanaei D, Ali I & Bhatnagar A, *J Mol Liq*, 215 (2016) 671.

20 Jin G P, Xu S Y, Lei P, Fu Y, Feng X, Wu Z X, Yu M, Dai S & Liu G, *Electrochim Acta*, 130 (2014) 526.

21 Zuin V G, Yariwake J H & Bicchi C, *J Chromatogr A*, 985 (2003) 159.

22 Qin S J & Yan B, *Anal Chim Acta*, 1012 (2018) 82.

23 Bon V, Kavoosi N, Senkovska I, Müller P, Schaber J, Wallacher D, Többens D M, Müller U & Kaske S, *Dalton Trans*, 45 (2016) 4407.

24 Gao E J & Liu Q T, *J Struct Chem*, 51 (2010) 1132.

25 Gao E J, Sun T D, Liu S H, Ma S, Wen Z, Wang Y, Zhu M C, Wang L, Gao X N, Guan F, Guo M J & Liu F C, *Eur J Med Chem*, 45 (2010) 4531.

26 Duan H, Zeng Y F, Yao X, Xing P Y, Liu J & Zhao Y L, *Chem Mater*, 29 (2017) 3671.

27 Sheldrick G M, SADABS, University of Göttingen, Göttingen, Germany, 1996.

28 Bruker AXS, SAINT software Reference Manual, Madison, WI, 1998.

29 (a) Sheldrick G M, *SHELXL-97, Program for X-ray Crystal Structure Refinement*, Göttingen University, Göttingen, Germany, 1997; (b) Sheldrick G M, *Crystal structure refinement with SHELXL*, *Acta Cryst,* C71 (2015) 3.

30 Nakamoto K, *Infrared and Raman Spectra of Inorganic and Coordination Compounds*, 4th edn, Wiley Press, New York, 1986.

31 (a) Yang E C, Zhao H K, Ding B, Wang X G & Zhao X J, *Cryst Growth Des,* 7 (2007) 2009; (b) Li Y, Yu J W, Liu Z Y, Yang E C & Zhao X J, *Inorg Chem*, 54 (2015) 153.

32 Thomas S W, Joly G D & Swager T M, *Chem Rev*, 107 (2007) 1339.